

Brain-Gen: Towards Interpreting Neural Signals for Stimulus Reconstruction Using Transformers and Latent Diffusion Models

Hasib Aslam^{a,*}, Muhammad Talal Faiz^{a,*}, Muhammad Imran Malik^{a,**}

^a*School of Electrical Engineering and Computer Science, National University of Sciences and Technology (NUST), H-12, Islamabad, 44000, Islamabad, Pakistan*

Abstract

Advances in neuroscience and artificial intelligence have enabled preliminary decoding of brain activity. However, despite the progress, the interpretability of neural representations remains limited. A significant challenge arises from the intrinsic properties of electroencephalography (EEG) signals, including high noise levels, spatial diffusion, and pronounced temporal variability. To interpret the neural mechanism underlying thoughts, we propose a transformers-based framework to extract spatial-temporal representations associated with observed visual stimuli from EEG recordings. These features are subsequently incorporated into the attention mechanisms of Latent Diffusion Models (LDMs) to facilitate the reconstruction of visual stimuli from brain activity. The quantitative evaluations on publicly available benchmark datasets demonstrate that the proposed method excels at modeling the semantic structures from EEG signals; achieving up to 6.5% increase in latent space clustering accuracy and 11.8% increase in zero shot generalization across unseen classes while having comparable Inception Score and Fréchet Inception Distance with existing baselines. Our work marks a significant step towards generalizable semantic interpretation of the EEG signals.

Keywords: Human Computer Interaction, Neural signal interpretability, Visual stimulus reconstruction, Generative modeling from EEG

1. Introduction

The inner working of the human brain is an intriguing open research question, drawing attention of scientists across disciplines, from neuroscience to computer science. Each field approaches this conundrum with their own motivation ranging from advancing biologically plausible computational cognition models to gaining inspiration for development of intelligent machines.

*Equal Contribution.

**Corresponding author.

Email addresses: `haslam.bs21seecs@seecs.edu.pk` (Hasib Aslam),
`mfaiz.bs21seecs@seecs.edu.pk` (Muhammad Talal Faiz), `malik.imran@seecs.edu.pk` (Muhammad Imran Malik)

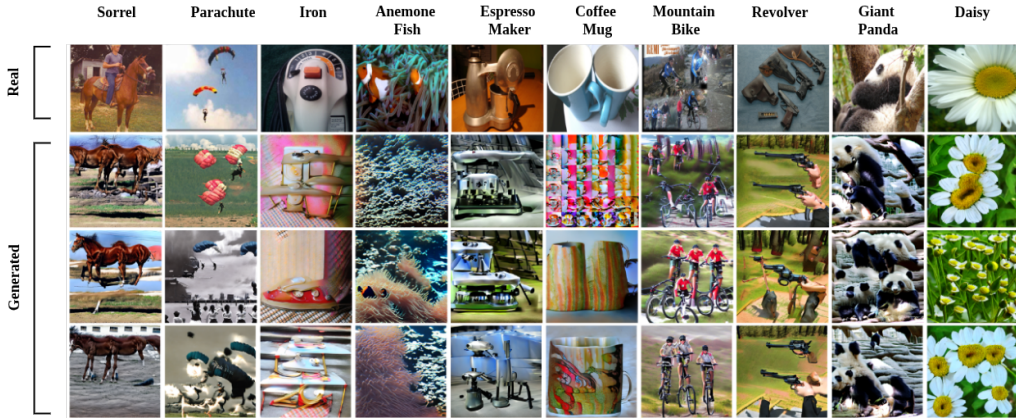


Figure 1: Image generation results from EEG signals corresponding to first 10 classes of EEG-CVPR40 dataset 5.1.1 from test split. The first row illustrates ground-truth images shown to the subject with the latter rows consisting of reconstructions, using subject’s EEG.

Over the past decade, development in Neuroimaging techniques such as functional Magnetic Resonance Imaging (fMRI) and ElectroEncephaloGraph (EEG) have given us valuable insights into cognitive processes consequently fueling numerous studies [1, 2].

Computational approaches such as Deep Neural Networks (DNNs) have significantly accelerated these studies. They have proven to be a powerful tool for decoding brain signals and engendering numerous applications in brain-computer interfaces (BCI) [3]. In particular the use of EEG signals has been extended to many medical applications such as assistive technologies [4, 5], rehabilitation [6, 7], motor function support [8], as well as to non-medical domains including drowsiness detection [9], entertainment and gaming [10].

Moreover, recent studies suggest that brain signals contain cues corresponding to visual and linguistic cognition [11, 12, 13]. A notable breakthrough demonstrated that brain-signals contain explicit visual cues from thoughts that can be used for reconstructing semantically relevant visuals [14]. This opens up the possibility of generating images depicting one’s thoughts using EEG signals. These findings inspire the objectives of our work.

This research aims to expand the capabilities of visual stimulus reconstruction using EEG data acquired from the cerebral cortex in response to specific image-based visual stimuli. Although most work in this area utilizes fMRI for its high spatial resolution, EEG was selected for this particular study, as it is more cost-effective and portable method, offering a higher temporal resolution thus capturing the instantaneous bio-electric activity via scalp electrodes. However, EEG presents unique challenges [2]. EEG signals are spatially diffused resulting in distorted recordings through the skull and scalp. Consequently, accurately locating the signal source is challenging. Lastly, EEG data is inherently noisy, susceptible to movement artifacts, and exhibits a low signal-to-noise ratio [15], further complicating the decoding process.

This work leverages the modeling capabilities of deep neural networks to learn semantically rich representations of EEG signals for reconstructing associated visual stimuli.

To address the apparent disparity between the two data modalities involved - static, two-dimensional visual stimuli and dynamic, multi-channel EEG time-series signals, we employ a two-stage framework. The key steps are: (i) train a deep neural network to learn EEG signal representations and (ii) reconstruct the image using a diffusion model guided by the learned EEG latents. In this paper, we make the following contributions:

- We propose a largely unexplored transformer based architecture with explicit focus on both spatial and temporal dynamics of EEG signals, which enhances the semantic structure of our latent space.
- We test the proposed framework on benchmark datasets for downstream tasks of classification, clustering, stimulus reconstruction and class generalization, where it outperforms most existing baselines.

2. Related Work

This section reviews the recent approaches relevant to generating images from EEG signals. Analogous to the standard structure for text-to-image generation [16], our literature review and consequently the EEG-to-Image reconstruction pipeline consists of two core processes: (i) Encoding raw signals into semantic representations and (ii) Decoding these embeddings into realistic images. This two-fold review serves as the backdrop for understanding the structure and rationale of our approach.

2.1. Encoding EEG Signals

Depending on the application domain and the scope of analysis, EEG signal interpretation techniques can generally be categorized into two broad approaches. The first approach frames EEG interpretation as a classification problem, wherein the objective is to assign each signal to a corresponding class label. Representative studies include [17, 18, 19, 20]. Secondly, it is also common to explicitly extract features from EEG signals at this stage and use them for down stream applications [21, 22, 23, 24]. These aforementioned works have either used contrastive learning [21, 22, 23], or masked signal modeling [24] as training objectives. While it is also possible to use a combination of both methods [25]. Regardless of the problem setup, most of the stated studies have either used Convolutional Neural Networks [26, 25] or LSTMs, as in [17, 20, 22, 19], or combination of both [18], as backbone architectures of their encoders, while some such as [24] have used the architecture similar to ViTLarge [27] as the encoder backbone.

2.2. Decoding Image From Encoded EEG

Reconstruction of visual stimuli from EEG signals is commonly achieved through generative models such as Generative Adversarial Networks (GANs) and Variational Autoencoders (VAEs). These models learn a conditional map from the latent space of EEG features to the pixel space of corresponding images [28]. However, the scarcity of paired EEG-image data limits this approach as effectively training generative models requires a lot of data.

To enhance image generation quality, GAN variants such as cProGAN [29] with additional convolution layers have been used, improving image resolution [19]. DCLS-GAN is another variant that produces images from both noise vector as well as the combined

description vector [30]. EEGStyleGAN-ADA proposed by Singh et al. [23] extends [31] by incorporating adaptive augmentation on images before passing them to discriminator to overcome the deficiency of large datasets. In addition to the widespread use of GANs, several works [24, 32, 33, 34] have employed diffusion models [35] for image generation, achieving superior quantitative and qualitative performance.

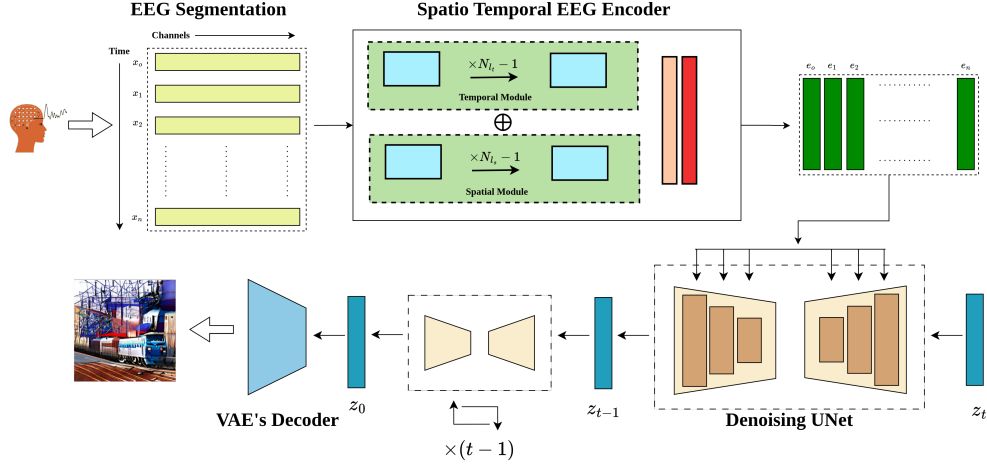


Figure 2: System Diagram: First we use sliding window segmentation to extract multiple, sub samples from an EEG signal. Each of the sub sample is then encoded independently by the spatio-temporal encoder. The resulting sequence of EEG representations is then used to condition the reverse diffusion process of the Stable Diffusion, resulting in semantically aligned reconstruction of the visual stimuli.

3. Methodology

This section presents our proposed framework for learning semantically rich representations of EEG signals and generating relevant images. We use a conditioning mechanism that integrates EEG latents into the diffusion process, generating images and forming our reconstruction pipeline. Below, we detail the problem statement, key components and individual processes for this task.

3.1. Problem Statement

Let set D be a collection of n unique pairs of EEG signals, images, and corresponding images class labels, represented as

$$D = \{(x_i, q_i, y_i)\}_{i=1}^n$$

such that $x_i \in \mathbb{R}^{t \times c}$, $y_i \in \mathbb{R}^{w \times h \times 3}$ and $q_i \in \mathbb{R}$ where c, t represents the number of channels and number of time steps in the EEG signal, respectively and w, h represent the width and height of the original image. Our goal is to find a parameterized function f_θ that maps x_i to y_i for $i = 1, \dots, n$, where θ denotes the learnable parameters.

Simply, our objective is to use EEG signals recorded while exposing subjects to visual stimuli and achieve semantically aligned regeneration of original images.

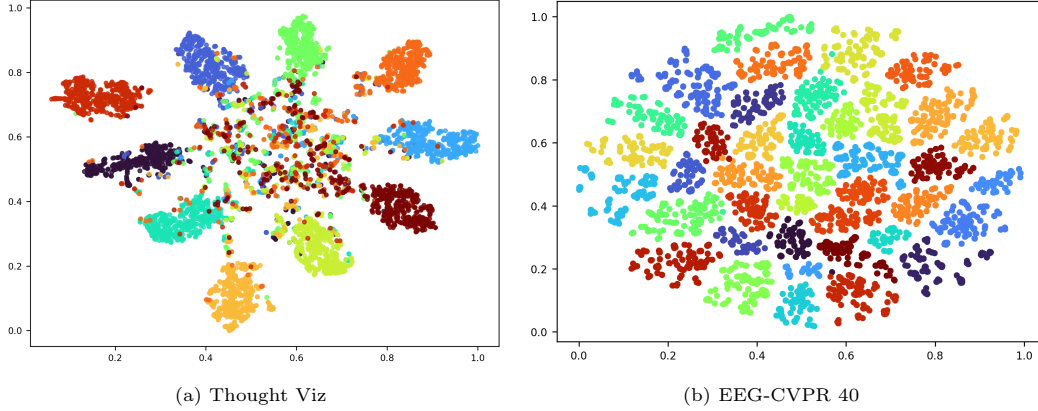


Figure 3: Visualization of features extracted by proposed encoder from unseen samples from ThoughtViz dataset in left column and EEG-CVPR40 in right column using TSNE plots.

3.2. Spatio-Temporal EEG Encoder

The first component of our proposed framework is a Spatio-Temporal encoder. To obtain feature rich embeddings we create a design that (i) captures long-range temporal dependencies, (ii) models spatial relationships across channels, and (iii) preserves both local and global contextual information. Existing approaches rely predominantly on CNNs and RNN variants such as LSTMs, each with inherent limitations for this objective.

CNNs are primarily designed to extract hierarchal features from grid structures such as images. Their application on time-series data such as EEG requires rearranging the signal into a 2-dimensional grid, with channels on one axis and discrete time samples on the other. Next, successive filters of varying sizes are applied on the grid to extract spatial information. As the filters operate on localized patches in this grid, their ability to capture dependencies across time or channels becomes limited. Consequently, capturing global dependencies requires large receptive fields and deep filter stacks whose computational cost scales non-linearly with model depth and input length.

In contrast, RNNs in general and specifically LSTMs are well suited for processing time signals because of their ability to capture long term dependencies. At each time step RNN units can access discrete values from all channels, when the channel dimension is considered as the feature dimension thus learning the necessary dependencies. However, the sequential processing in RNNs lacks an explicit mechanism for attending to all time steps simultaneously, leading to limited global temporal awareness.

To solve the issues discussed above, we take our inspiration from work on EEG based authentication systems [36], where transformer based architecture, incorporating explicit spatial and temporal modules, is employed for classification of the subject’s EEG signal. We adapt the proposed architecture to a contrastive learning framework, learning discriminative features instead of class labels. Through experiments we establish the sufficiency of the temporal module for low complexity, downstream tasks such as that of classification and clustering. However, for stimulus reconstruction, we observe significant performance gains when the spatial module is also included. *See 5.3 for more.* The general architecture of the encoder is given below.

3.2.1. Temporal Encoder

The temporal encoder processes EEG signals across time, preserving temporal dependencies. The temporal encoding of an input $x_i \in \mathbb{R}^{t \times c}$ is computed as:

$$\begin{aligned} x_t &= E_t(x_i) \\ E_t &: \mathbb{R}^{t \times c} \rightarrow \mathbb{R}^{t \times c} \end{aligned}$$

where $E_t(\cdot)$ represents a multi-layered, multi-head self-attention transformer block, with N_{l_t} layers, each with N_{h_t} heads, c is the number of electrodes used for recording EEG and t defines the number of time steps in the sample.

3.2.2. Spatial Encoder

The spatial encoder captures correlations among EEG channels by applying a transformer-based model along the channel dimension. Given the feature encoding from the temporal encoder $x_t \in \mathbb{R}^{t \times c}$ the representation obtained is as follows:

$$\begin{aligned} x_s &= E_s(x_t^T) \\ E_s &: \mathbb{R}^{c \times t} \rightarrow \mathbb{R}^{c \times t} \end{aligned}$$

where x^T represents the transpose of x and $E_s(\cdot)$ represents a multi-layered, multi-head self-attention transformer block, with N_{l_s} layers, each with N_{h_s} heads, t is the sequence length, and c is the number channels in EEG signal.

3.2.3. Latent Projection

The final representation is obtained by flattening the combined spatial and temporal embeddings and projecting them into a lower-dimensional latent space using a fully connected network.

$$\begin{aligned} z &= F(x_s) \\ F &: \mathbb{R}^{t \times c} \rightarrow \mathbb{R}^{1 \times d} \end{aligned}$$

where F consists of fully connected layers with dropout regularization, preceded by the flattening operation. So in its final form our encoder is defined as $E_\theta(\cdot) = F(E_s(E_t(\cdot)))$ such that $E_\theta : \mathbb{R}^{t \times c} \rightarrow \mathbb{R}^{1 \times d}$

4. Contrastive Learning

We optimize the encoder using a contrastive objective based on triplet loss [37]. The goal is to learn representations that remain consistent across EEG signals corresponding to the same image while separating representations from different images. We define the margin-based triplet loss as:

$$\mathcal{L}_{\text{triplet}} = \max(d(E_\theta(x_a), E_\theta(x_p)) - d(E_\theta(x_a), E_\theta(x_n)) + \beta, 0), \quad \beta = 0.05,$$

where $q_a = q_p$ and $q_a \neq q_n$, and $d(\cdot, \cdot)$ denotes cosine distance.

To improve training stability and promote better separation between classes, we employ semi-hard negative mining, selecting negatives that satisfy

$$\begin{aligned} d(E_\theta(x_a), E_\theta(x_p)) &< d(E_\theta(x_a), E_\theta(x_n)) \\ &< d(E_\theta(x_a), E_\theta(x_p)) + \alpha, \end{aligned}$$

with $\alpha = 0.1$. Selecting negatives that are harder than easy examples, but still lie within the margin defined by the anchor to positive distance.

4.1. EEG Signal Tokenization

To make the feature extracted from EEG signals compatible with the conditioning mechanism of stable diffusion, which expects sequence of embeddings from textual prompt, we use the sliding window approach to extract multiple sub samples, each of which is treated as an individual token and is processed independently. Let an EEG recording be $x \in \mathbb{R}^{t \times c}$, where t is the number of time steps and c the number of channels. We define a sliding-window extraction operator with window length l and stride s where the number of extracted segments n is:

$$n = \left\lfloor \frac{t-l}{s} \right\rfloor + 1.$$

Each windowed segment is

$$x_i = x[t_i : t_i + l - 1] \in \mathbb{R}^{l \times c}, \quad i = 1, \dots, n,$$

with

$$t_i = (i - 1)s.$$

Each segment is independently mapped by the EEG encoder

$$E_\theta : \mathbb{R}^{l \times c} \rightarrow \mathbb{R}^d.$$

Thus, each token embedding is

$$e_i = E_\theta(x_i) \in \mathbb{R}^{1 \times d}.$$

Collecting all embeddings yields the final token sequence

$$S_t = [e_1, e_2, \dots, e_n] \in \mathbb{R}^{n \times d}.$$

4.2. Image Generation

We employ Stable Diffusion-2 [38] for image reconstruction task, through conditioning the reverse diffusion process on features extracted from EEG signals using the cross-attention mechanism [39]. Specifically we use the $S_t \in \mathbb{R}^{n \times d}$, the sequence of EEG features obtained from tokenization based approach described above, to replace the embedding sequence from textual prompt in traditional Stable Diffusion-2 [38] pipeline. Here the cross-attention is calculated as:

$$\text{Attention}(Q, K, V) = \text{softmax}\left(\frac{QK^\top}{\sqrt{d}}\right) V,$$

where the learnable projection matrices

$$W_Q^{(i)} \in \mathbb{R}^{d \times h}, \quad W_K^{(i)} \in \mathbb{R}^{d \times h}, \quad \text{and} \quad W_V^{(i)} \in \mathbb{R}^{d \times h}$$

are used to compute

$$Q = W_Q^{(i)} \cdot \phi_i(z_t), \quad K = W_K^{(i)} \cdot S_t, \quad V = W_V^{(i)} \cdot S_t.$$

Here, $\phi_i(z_t) \in \mathbb{R}^{N \times d_i}$ denotes the intermediate representation of the UNet implementing ϕ_θ . Based on EEG-Image conditioning pairs, we then learn the conditional LDM via

$$\mathcal{L}_{\text{LDM}} := \mathbb{E}_{x,y,\epsilon \sim \mathcal{N}(0,1)} \left[\left\| \epsilon - \epsilon_\theta(z_t, t, S_t) \right\|_2^2 \right], \quad (3)$$

where S_t is obtained from EEG encoder. To prevent overfitting of the EEG encoder for the image generation process, we use its weights from the contrastive learning task and keep them frozen. We finetune only the denoising UNet ϵ_θ , so that it learns the semantics in the latent space of EEG encoder. We start the training from the publicly available weights of Stable Diffusion 2.

5. Experiments and Results

In this section we discuss our experiments in detail. Alongside quantitative and qualitative results, we also compare with previous works to show the efficacy of our method.

5.1. Datasets

5.1.1. EEG-CVPR40

This dataset introduced in [17] consists of images from 40 ImageNet [40] classes where 50 samples of images are drawn from each class. The resulting 2000 samples are shown to each of six different subjects for 0.5 seconds, and the EEG signals are recorded at a sampling rate of 1 kHz. It results in 12000 samples in total, out of which 36 samples were discarded by the original authors. They also cut down the remaining 11964 samples to 440 time steps. To keep our work comparable, we use the raw dataset with the same train, validation, and test splits as provided in the original work. Finally in our work, we use the sliding window approach to create multiple sub-sample from each original sample. This is done independently in each of train, validation and test splits to ensure that there is no data leakage.

5.1.2. Thought Viz

This dataset first used in [21] for EEG to Image generation task is a limited dataset in which 23 subjects were shown images belonging to 10 different classes of ImageNet [40] and the EEG signals using 14 channels were recorded at sampling frequency of 2048 Hz and later down sampled to 128 Hz. The publicly available dataset contains 45390 train and 5706 test samples each containing 32 time steps from 14 channels, paired with class labels of original images that were shown to the subjects. Unlike EEG-CVPR40, this dataset only contains EEG signal to image class mappings. Consequently, due to the lack of pixel level information about the original image, this dataset is only used to test the generalization abilities of our proposed EEG encoder and not for image generation.

5.2. Evaluation Metrics

5.2.1. EEG K-Means Clustering Accuracy

To assess the strength of the features extracted by our *Spatio-Temporal Encoder*, we consider the accuracy of k-means clustering over features extracted from EEG signals. We take k , i.e, number of means to be the same as the number of classes in the dataset which are 40 and 10 in EEG-CVPR40 and ThoughtViz datasets respectively.

5.2.2. Zero Shot Class Generalization

To assess the generalization abilities of the proposed encoder across different classes, we train the encoder on a subset of classes and examine its feature extraction on remaining classes using k-means clustering, where k is set to the number of held out classes. To make our work comparable we keep the experimental setting similar to existing works [41, 23] where for training the encoder, samples from 34 classes are used and during testing k-means clustering is performed on the features extracted from samples belonging to the 6 held out classes.

5.2.3. Classification Accuracy

Even though, the proposed approach is based on a contrastive learning framework with the final goal being stimulus reconstruction, we evaluate the proposed encoder on the downstream task of predicting the class labels of the images shown to the subject corresponding to the EEG signal (classification). After the proposed encoder has been trained using the contrastive learning objective, a classification head consisting of full connected layers is added on top of the trained encoder. This head is trained using cross-entropy loss while keeping the weights of the base encoder frozen.

5.2.4. Inception score (IS)

To estimate the quality of images generated from EEG signals, we use the Inception Score [42], which provides a measure of the distinctiveness and sharpness of generated images. Using logits from Inception-V3 [43]. The Inception Score is defined as:

$$\text{IS}(G) = \exp \left(\mathbb{E}_{\mathbf{x} \sim p_g} [D_{\text{KL}}(p(y|\mathbf{x})||p(y))] \right), \quad (1)$$

where \mathbf{x} is a generated image, $p(y|\mathbf{x})$ is the conditional label distribution predicted by the Inception network, and $p(y) = \int p(y|\mathbf{x})p_g(\mathbf{x})d\mathbf{x}$ is the marginal distribution over all generated images. A higher IS indicates that the generated images are both diverse (i.e., $p(y)$ has high entropy) and meaningful (i.e., $p(y|\mathbf{x})$ is peaked).

5.2.5. Fréchet Inception Distance (FID)

To measure the similarity between the distribution of generated images and real ones, we use Fréchet Inception Distance (FID) [44]. We use the pre-trained Inception-V3 [43] model’s final pooling layer to extract a 2048-dimensional feature vector for each image. The FID is then computed between the multivariate Gaussians fitted to these feature representations of real and generated images as follows:

$$\text{FID}(r, g) = \|\mu_r - \mu_g\|_2^2 + \text{Tr} \left(\Sigma_r + \Sigma_g - 2(\Sigma_r \Sigma_g)^{1/2} \right), \quad (2)$$

where μ_r and Σ_r are the mean and covariance of the features for real images, and μ_g and Σ_g are those for generated images. A lower FID indicates that the generated images are more similar to the real ones in terms of both quality and diversity.

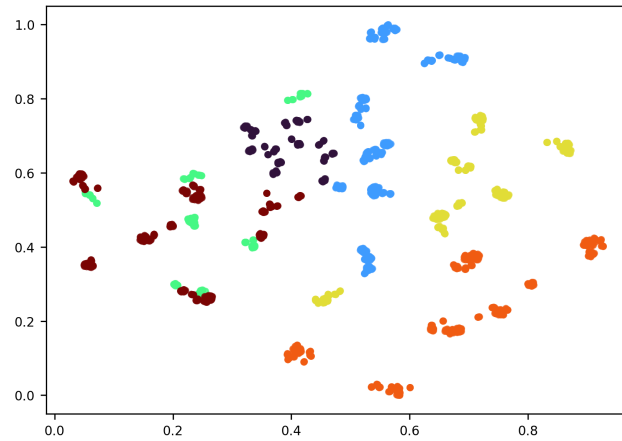


Figure 4: Visualization of features extracted by the proposed encoder from samples of unseen classes from EEG-CVPR40 using t-SNE.

Table 1: Classification and K Means Accuracies on ThoughtViz and EEG-CVPR40

Model	Classification Acc (%)	K Means Acc (%)
ThoughtViz		
ThoughtViz [21]	0.72	0.18
SiameseCNN [25]	0.779	–
EEG2Image [22]	0.55	0.52
EEGStyleGAN-ADA [23]	0.74	0.721
Ours	0.767	0.768
EEG-CVPR40		
LSTM Encoder [17]	0.829	0.45
DML [45]	0.977	–
LSTM-CNN [18]	0.944	–
BioLSTM [20]	0.991	–
NeuroVision [19]	0.988	–
EEGStyleGAN-ADA [23]	0.983	0.961
Ours	0.994	0.995

5.3. Results

5.3.1. EEG Encoding Results on ThoughtViz and EEG-CVPR40

In Table 1, classification accuracy and k-means accuracy of EEG signals from test splits of both datasets is presented. Relative to existing baselines our proposed encoder achieves an increase of 6.51% and 3.53% in the k-means accuracy on ThoughtViz and EEG-CVPR40 dataset respectively. For EEG-CVPR40 dataset the proposed encoder achieved highest classification accuracy 0.994, while the classification results on ThoughtViz remain comparable to the best performing architectures..

For EEG-CVPR40 dataset 5.1.1, the results were obtained by training the proposed architecture 3.2 with $N_{l_t} = 2$ and $H_{l_t} = 4$ and $N_{l_s} = 0$, *using only the temporal module*, with sequence length of $t = 32$ on contrastive learning objective, with hidden dimension $d = 128$, for 1024 epochs, with constant learning rate of $3e - 5$ using the Adam optimizer. The choice of hyper-parameters for encoder modules and signal length used are discussed in Appendix A and Appendix B respectively.

For ThoughtViz dataset 5.1.2, the results were obtained by training the proposed architecture 3.2 with $N_{l_t} = 2$ and $H_{l_t} = 2$ and $N_{l_s} = 0$, *using only the temporal module*, with sequence length of $t = 32$ on contrastive learning objective, with hidden dimension $d = 128$, for 4096 epochs, with constant learning rate of $3e - 5$ using the Adam optimizer.

5.3.2. Zero Shot Class Generalization

Table 2 shows the performance of proposed encoder on class generalization task on EEG-CVPR40 dataset and its comparison with existing baselines. Our methods achieved k-means clustering accuracy of 69.9% on features extracted from unseen classes, which is 11.84% higher, relative to previously reported results. Moreover for comparison, KNN accuracy is computed where relative gain of 15.11% is observed.

The results were obtained by training the proposed architecture 3.2 with $N_{l_t} = 2$ and $N_{h_t} = 4$ and $N_{l_s} = 0$, *using only the temporal module*, with sequence length of $t = 32$ on contrastive learning objective, with hidden dimension $d = 128$, for 60 epochs, with constant learning rate of $3e - 5$ using the Adam optimizer and testing on remaining 6 classes, the excluded set of classes was kept same as in [41, 23].

5.3.3. Image Generation Results on EEG-CVPR40

The quantitative results of proposed methodology on EEG-CVPR40 dataset are presented in Table 3 while qualitative results displayed in Figure 1. Comparable to existing baseline [34], the proposed method achieves Inception Score of 25.15 and Fréchet Inception Distance of 81.07.

We stress upon the need of both IS and FID for the accurate assessment of the stimulus reconstruction. IS is important as it is the measure of the visual quality of the generated images. The low values of IS are indication of the lack of diversity in generated population of images or the lack of semantic clarity in them, however any image generation model capable of generating high quality, diverse images will have high IS, regardless of their relevance with original visual stimuli. That’s why it is necessary to define some metric, like FID that measures semantic similarity between the distribution of generated and real images. Smaller FID means that the generated images are closer to original ones and vice versa.

Table 2: KNN and K-means clustering accuracies on the EEG-CVPR40 dataset for zero shot class generalization.

Model	SVM	KNN	K-Means
Cogni-Net [41]	0.78	0.72	-
EEGStyleGAN-ADA [23]	0.93	0.86	0.625
Ours	-	0.997	0.699

Table 3: FID and IS scores on the EEG-CVPR40 dataset.

Model	IS	FID
Brain2Image (GAN) [28]	5.07	-
Neurovision [19]	5.15	-
DCLS-GAN [30]	6.64	-
EEGStyleGAN-ADA [23]	10.82	174.13
DM-RE2I [32]	12.55	-
NeuroDM [33]	15.89	-
GWIT [34]	33.87	78.11
Ours	25.15	81.07

The results discussed above are obtained by finetuning the Stable Diffusion on EEG-CVPR40 dataset 5.1.1 following the method explained in 4.2. While finetuning, the generation was conditioned on features extracted through tokenization encoding of the corresponding EEG signals 4.1. We used the constant learning rate of $1e-5$ and finetuned the model for 25000 steps. Notably, we observe that image generation quality increases with increase in complexity of encoder. *See Appendix C for details.* We pre-trained the proposed EEG encoder with $N_{l_s} = 6$, $N_{l_t} = 6$, $N_{h_s} = 8$ and $N_{h_t} = 8$ using both the temporal and spatial modules, with sequence length $t = 64$ on contrastive learning objective, with hidden dimension $d = 1024$ to match the latent space of stable diffusion.

6. Acknowledgment

The authors declare no conflict of interest.

References

- [1] K. Uğurbil, Development of functional imaging in the human brain (fmri); the university of minnesota experience, *Neuroimage* 62 (2) (2012) 613–619.
- [2] M. D. Nunez, P. L. Nunez, R. Srinivasan, Electroencephalography (eeg): Neurophysics, experimental methods, and signal processing, in: H. Ombao, M. Linquist, W. Thompson, J. Aston (Eds.), *Handbook of Neuroimaging Data Analysis*, Chapman & Hall/CRC, 2016, pp. 175–197. doi:10.13140/rg.2.2.12706.63687.
- [3] R. T. Schirrmeister, J. T. Springenberg, L. D. J. Fiederer, M. Glasstetter, K. Eggenasperger, M. Tangermann, F. Hutter, W. Burgard, T. Ball, Deep learning

- with convolutional neural networks for eeg decoding and visualization, in: Human Brain Mapping, 2017.
URL <https://api.semanticscholar.org/CorpusID:1348207>
- [4] J. Li, et al., Towards bci-actuated smart wheelchair system, Biomedical Engineering Online Describes a brain-actuated smart wheelchair system using P300-based BCI for rehabilitation of severely motor disabled individuals (8 2018).
URL <https://pmc.ncbi.nlm.nih.gov/articles/PMC6102906/>
- [5] L. A. Farwell, E. Donchin, Talking off the top of your head: toward a mental prosthesis utilizing event-related brain potentials, *Electroencephalography and clinical Neurophysiology* 70 (6) (1988) 510–523.
- [6] K. Värbu, N. Muhammad, Y. Muhammad, Past, present, and future of eeg-based bci applications, *Sensors* 22 (9) (2022) 3331.
- [7] L. Zhang, et al., A review of eeg-based brain-computer interface systems design, *Brain Science Advances* 4 (2), comprehensive review of BCI paradigms, signal processing methods, and feature extraction techniques (12 2018). doi:10.26599/BSA.2018.9050010.
- [8] C. Neuper, G. R. Müller-Putz, R. Scherer, G. Pfurtscheller, Motor imagery and eeg-based control of spelling devices and neuroprostheses, *Progress in brain research* 159 (2006) 393–409.
- [9] C.-T. Lin, C.-J. Chang, B.-S. Lin, S.-H. Hung, C.-F. Chao, I.-J. Wang, A real-time wireless brain-computer interface system for drowsiness detection, *IEEE Transactions on Biomedical Circuits and Systems* 4 (4) (2010) 214–222. doi:10.1109/TBCAS.2010.2046415.
- [10] N. Thomasson, An introduction to bci and its use in video games: A review, *Journal of Student Research* 12 (1) (2 2023). doi:10.47611/jsrhs.v12i1.3924.
URL <https://www.jsr.org/hs/index.php/path/article/view/3924>
- [11] S. Weiss, H. M. Mueller, The contribution of eeg coherence to the investigation of language, *Brain and Language* 85 (2) (2003) 325–343. doi:[https://doi.org/10.1016/S0093-934X\(03\)00067-1](https://doi.org/10.1016/S0093-934X(03)00067-1).
URL <https://www.sciencedirect.com/science/article/pii/S0093934X03000671>
- [12] P. M. Alday, M/eeg analysis of naturalistic stories: a review from speech to language processing, *Language, Cognition and Neuroscience* 34 (4) (2019) 457–473. arXiv:<https://doi.org/10.1080/23273798.2018.1546882>, doi:10.1080/23273798.2018.1546882.
URL <https://doi.org/10.1080/23273798.2018.1546882>
- [13] M. Gillis, J. Vanthornhout, J. Z. Simon, T. Francart, C. Brodbeck, Neural markers of speech comprehension: Measuring eeg tracking of linguistic speech representations, controlling the speech acoustics, *Journal of Neuroscience* 41 (50) (2021) 10316–10329. arXiv:<https://www.jneurosci.org/content/41/50/10316.full.pdf>, doi:10.1523/JNEUROSCI.0812-21.2021.
URL <https://www.jneurosci.org/content/41/50/10316>

- [14] Kyoto University, Take a look, and you'll see, into your imagination: Using fmri signals and deep neural network ai to decode and predict what a subject is seeing or imagining, ScienceDaily (May 2017).
URL <https://www.sciencedaily.com/releases/2017/05/170531094850.htm>
- [15] S. Sadiya, T. Alhanai, M. M. Ghassemi, Artifact detection and correction in eeg data: A review, arXiv preprint arXiv:2106.13081Discusses that EEG is inherently noisy, susceptible to movement artifacts, and exhibits a low signal-to-noise ratio, complicating decoding. (2021).
URL <https://arxiv.org/abs/2106.13081>
- [16] N. Hussen, A. Samir, A. Adel, A. Gaber, M. Attaia, A. Mohamed, Advancing creativity: A comprehensive review of ai-driven text-to-image generation and its applications, *Advanced Sciences and Technology Journal* 2 (2) (2025) 1–17.
- [17] C. Spampinato, S. Palazzo, I. Kavasidis, D. Giordano, N. Souly, M. Shah, Deep learning human mind for automated visual classification, in: *Proceedings of the IEEE conference on computer vision and pattern recognition*, 2017, pp. 6809–6817.
- [18] X. Zheng, W. Chen, M. Li, T. Zhang, Y. You, Y. Jiang, Decoding human brain activity with deep learning, *Biomedical Signal Processing and Control* 56 (2020) 101730.
- [19] S. Khare, R. N. Choubey, L. Amar, V. Udutalapalli, Neurovision: perceived image regeneration using cprogan, *Neural Computing and Applications* 34 (8) (2022) 5979–5991.
- [20] J. Jiang, A. Fares, S.-H. Zhong, A brain-media deep framework towards seeing imaginations inside brains, *IEEE Transactions on Multimedia* 23 (2020) 1454–1465.
- [21] P. Tirupattur, Y. S. Rawat, C. Spampinato, M. Shah, Thoughtviz: Visualizing human thoughts using generative adversarial network, in: *Proceedings of the 26th ACM international conference on Multimedia*, 2018, pp. 950–958.
- [22] P. Singh, P. Pandey, K. Miyapuram, S. Raman, Eeg2image: image reconstruction from eeg brain signals, in: *ICASSP 2023-2023 IEEE International Conference on Acoustics, Speech and Signal Processing (ICASSP)*, IEEE, 2023, pp. 1–5.
- [23] P. Singh, D. Dalal, G. Vashishtha, K. Miyapuram, S. Raman, Learning robust deep visual representations from eeg brain recordings, in: *Proceedings of the IEEE/CVF Winter Conference on Applications of Computer Vision*, 2024, pp. 7553–7562.
- [24] Y. Bai, X. Wang, Y.-p. Cao, Y. Ge, C. Yuan, Y. Shan, Dreamdiffusion: Generating high-quality images from brain eeg signals, arXiv preprint arXiv:2306.16934 (2023).
- [25] R. Mishra, A. Bhavsar, Eeg classification for visual brain decoding via metric learning., in: *Bioimaging*, 2021, pp. 160–167.
- [26] A. Krizhevsky, I. Sutskever, G. E. Hinton, Imagenet classification with deep convolutional neural networks, *Communications of the ACM* 60 (6) (2017) 84–90.

- [27] A. Dosovitskiy, L. Beyer, A. Kolesnikov, D. Weissenborn, X. Zhai, T. Unterthiner, M. Dehghani, M. Minderer, G. Heigold, S. Gelly, et al., An image is worth 16x16 words: Transformers for image recognition at scale, arXiv preprint arXiv:2010.11929 (2020).
- [28] I. Kavasidis, S. Palazzo, C. Spampinato, D. Giordano, M. Shah, Brain2image: Converting brain signals into images, in: Proceedings of the 25th ACM international conference on Multimedia, 2017, pp. 1809–1817.
- [29] T. Karras, T. Aila, S. Laine, J. Lehtinen, Progressive growing of gans for improved quality, stability, and variation (2018). arXiv:1710.10196.
URL <https://arxiv.org/abs/1710.10196>
- [30] A. Fares, S.-h. Zhong, J. Jiang, Brain-media: A dual conditioned and lateralization supported gan (dcls-gan) towards visualization of image-evoked brain activities, in: Proceedings of the 28th ACM International Conference on Multimedia, 2020, pp. 1764–1772.
- [31] T. Karras, M. Aittala, J. Hellsten, S. Laine, J. Lehtinen, T. Aila, Training generative adversarial networks with limited data, in: Advances in Neural Information Processing Systems, 2020.
URL <https://arxiv.org/abs/2006.06676>
- [32] H. Zeng, N. Xia, D. Qian, M. Hattori, C. Wang, W. Kong, Dm-re2i: A framework based on diffusion model for the reconstruction from eeg to image, Biomedical Signal Processing and Control 86 (2023) 105125.
- [33] D. Qian, H. Zeng, W. Cheng, Y. Liu, T. Bikki, J. Pan, Neurodm: Decoding and visualizing human brain activity with eeg-guided diffusion model, Computer Methods and Programs in Biomedicine 251 (2024) 108213.
- [34] E. Lopez, L. Sigillo, F. Colonnese, M. Panella, D. Comminiello, Guess what i think: Streamlined eeg-to-image generation with latent diffusion models, in: ICASSP 2025-2025 IEEE International Conference on Acoustics, Speech and Signal Processing (ICASSP), IEEE, 2025, pp. 1–5.
- [35] J. Ho, A. Jain, P. Abbeel, Denoising diffusion probabilistic models, arXiv preprint arXiv:2006.11239 (2020).
- [36] Y. Du, Y. Xu, X. Wang, L. Liu, P. Ma, Eeg temporal–spatial transformer for person identification, Scientific Reports 12 (1) (2022) 14378.
- [37] F. Schroff, D. Kalenichenko, J. Philbin, Facenet: A unified embedding for face recognition and clustering, in: Proceedings of the IEEE conference on computer vision and pattern recognition, 2015, pp. 815–823.
- [38] R. Rombach, A. Blattmann, D. Lorenz, P. Esser, B. Ommer, High-resolution image synthesis with latent diffusion models, in: Proceedings of the IEEE/CVF Conference on Computer Vision and Pattern Recognition (CVPR), 2022, pp. 10684–10695.

- [39] A. Vaswani, N. Shazeer, N. Parmar, J. Uszkoreit, L. Jones, A. N. Gomez, Ł. Kaiser, I. Polosukhin, Attention is all you need, *Advances in neural information processing systems* 30 (2017).
- [40] J. Deng, W. Dong, R. Socher, L.-J. Li, K. Li, L. Fei-Fei, Imagenet: A large-scale hierarchical image database, in: *2009 IEEE conference on computer vision and pattern recognition*, Ieee, 2009, pp. 248–255.
- [41] P. Mukherjee, A. Das, A. K. Bhunia, P. P. Roy, Cogni-net: Cognitive feature learning through deep visual perception, in: *2019 IEEE International Conference on Image Processing (ICIP)*, 2019, pp. 4539–4543. doi:10.1109/ICIP.2019.8803717.
- [42] T. Salimans, I. Goodfellow, W. Zaremba, V. Cheung, A. Radford, X. Chen, Improved techniques for training gans, *Advances in neural information processing systems* 29 (2016).
- [43] C. Szegedy, V. Vanhoucke, S. Ioffe, J. Shlens, Z. Wojna, Rethinking the inception architecture for computer vision, in: *Proceedings of the IEEE Conference on Computer Vision and Pattern Recognition (CVPR)*, 2016, pp. 2818–2826.
- [44] M. Heusel, H. Ramsauer, T. Unterthiner, B. Nessler, S. Hochreiter, Gans trained by a two time-scale update rule converge to a local nash equilibrium, in: I. Guyon, U. V. Luxburg, S. Bengio, H. Wallach, R. Fergus, S. Vishwanathan, R. Garnett (Eds.), *Advances in Neural Information Processing Systems*, Vol. 30, Curran Associates, Inc., 2017.
- [45] J. Jiang, A. Fares, S.-H. Zhong, A context-supported deep learning framework for multimodal brain imaging classification, *IEEE Transactions on Human-Machine Systems* 49 (6) (2019) 611–622.

Module	N_{l_t}	N_{h_t}	N_{l_s}	N_{h_s}	K-Means Acc(%)
Temporal	2	2	0	0	0.992
Temporal	2	4	0	0	0.993
Temporal	4	2	0	0	0.994
Temporal	4	4	0	0	0.994
Spatial	0	0	2	2	0.996
Spatial	0	0	2	4	0.996
Spatial	0	0	4	2	0.998
Spatial	0	0	4	4	0.998
Both	2	2	2	2	0.996
Both	2	4	2	4	0.996
Both	4	2	4	2	0.996
Both	4	4	4	4	0.997

Table A.4: Analyzing the change in K-means accuracy by adding or removing spatial and temporal modules in proposed encoder 3.2. The results are given for validation split of EEG-CVPR40 dataset. 5.1.1

Appendix A. Contributions of Temporal and Spatial Modules

To reveal the significance of spatial and temporal modules of our proposed EEG Encoder 3.2, we experiment in the settings where only one of the two modules is used for feature extraction. We keep the sequence length fixed to 64 for EEG-CVPR40 dataset 5.1.1 and 32 for ThoughtViz 5.1.2. Further for each module, we also vary the number of encoder layers and self attention heads, to quantify the relationship between complexity of the architecture and the quality of the features extracted. The results are given in Table A.4 and Table A.5 for EEG-CVPR40 and ThoughtViz dataset respectively.

For EEG-CVPR40 dataset, it can be seen that the validation k-means accuracy is not effected at all by the choice of the module in the proposed encoder. However in ThoughtViz dataset, the results are significantly better for same number of layers and heads if we use temporal module, as compared to the spatial one. Which hints that the class level discriminative features are fairly pronounced along both spatial and temporal views of the signals in EEG-CVPR40, but only along temporal dimension for the case of ThoughtViz.

Moreover the effect of increase or decreasing the individual number of layers and heads is observed to be negligible, signaling that feature space approximated by few layered transformers, is structured sufficiently good, at least for the immediate task of clustering and subsequently for that of classification. Based on these observations we opt to use only the temporal module, because it’s performance is satisfactory across both datasets, in main experiments and limit the number of layer and heads with $N_{l_s} = 2$ and $N_{h_s} = 4$.

Appendix B. Effect of Signal Length on Feature Extraction

The duration of EEG signal required for BCI tasks, directly determines the required computation resources and consequently its application in real world scenarios. Therefore we have explored the effect of signal duration on model’s performance to find the optimal duration for downstream tasks on EEG-CVPR40 dataset. We experimented with increasing signals duration starting from 32 to 256 time steps with identical hyper-parameters

Module	N_{l_t}	N_{h_t}	N_{l_s}	N_{h_s}	K-Means Acc(%)
Temporal	1	1	0	0	0.764
Temporal	1	2	0	0	0.758
Temporal	2	1	0	0	0.765
Temporal	2	2	0	0	0.767
Temporal	2	7	0	0	0.777
Spatial	0	0	1	1	0.405
Spatial	0	0	1	2	0.366
Spatial	0	0	2	1	0.658
Spatial	0	0	2	2	0.661
Spatial	0	0	2	8	0.670
Both	1	1	1	1	0.604
Both	1	2	1	2	0.682
Both	2	1	2	1	0.749
Both	2	2	2	2	0.715
Both	2	7	2	8	0.745

Table A.5: Analyzing the change in K-means accuracy by adding or removing spatial and temporal modules in proposed encoder 3.2. The results are given for validation split of ThoughtViz dataset. 5.1.1

on contrastive learning task. We evaluated the performance of proposed encoder using K-means clustering accuracy and classification accuracy over validation dataset and found it’s performance to be consistent even with reduced duration of signal, which shows the robustness of proposed methods. The results are presented in Table B.6. For better visualization the trend is also given in Figure B.5.

Table B.6: K-means clustering and classification across different sequence lengths on EEG-CVPR40 dataset

Seq. Len	Classification Acc (%)	K Means Acc (%)
32	0.993	0.995
64	0.992	0.994
96	0.993	0.994
128	0.987	0.991
160	0.988	0.993
192	0.989	0.993
224	0.986	0.989
256	0.985	0.991

Appendix C. Effect of Encoder’s Complexity on Image Generation

The image generation results reported in 5.3.3, use scaled up version of proposed EEG encoder 3.2, using both spatial and temporal modules. This choice is motivated by the empirical observation that increasing the encoders complexity, results in image

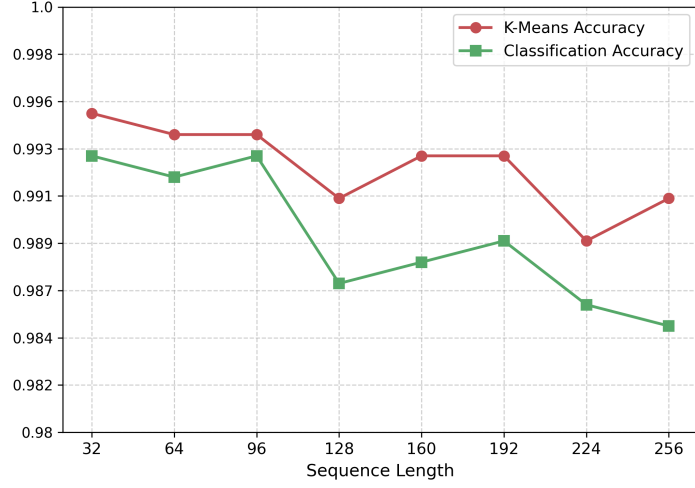


Figure B.5: Effect of sequence length on performance of proposed encoder on EEG-CVPR40 dataset.

generation with better FID and IS, even though the clustering accuracy remains similar, as explained in Appendix A.

For illustration, we experiment by pretraining a low complexity encoder, with $N_{l_t} = 2$, $N_{h_t} = 4$ and $N_{l_s} = 0$ using only the temporal module, with sequence length $t = 32$ on contrastive learning objective, with hidden dimension $d = 1024$. We then use this pretrained encoder to finetune the Stable Diffusion in the same manner as explained in 5.3.3. The resulting model's performance is far below than the previous one with, FID score of 245.93 and IS of 9.47, indicating the superiority of high representation abilities of the complex encoder with both spatial and temporal modules. Similar conclusion can be drawn through comparison of the visual quality of the generated images, when both temporal and spatial modules are employed, figure C.6 and when only temporal module is employed, figure C.7.

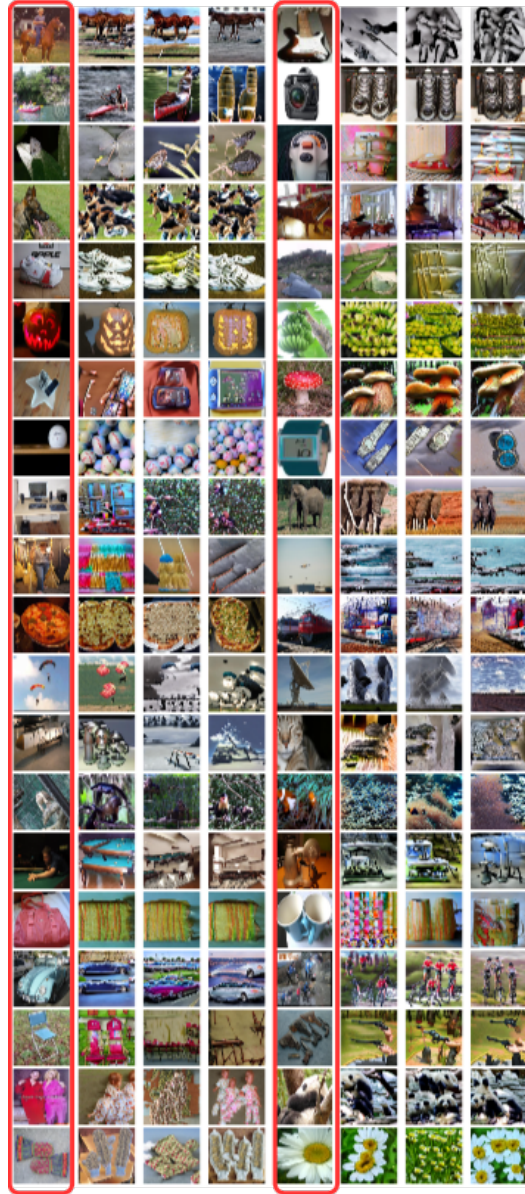


Figure C.6: Images generated by Stable diffusion through conditioning from scaled up version of the EEG encoder, using both spatial and temporal modules. Columns 1 and 4 show the ground truth images, while the adjacent columns display the reconstructed images from the corresponding class.

